Full Length Research Paper

Improving efficiency of inverse constitutive analysis of reinforced concrete flexural members

Viktor Gribniak*, Gintaris Kaklauskas, Rimantas Kacianauskas and Romualdas Kliukas

Vilnius Gediminas Technical University, Sauletekio 11, Vilnius LT-10223, Lithuania.

Adequate modeling of reinforced concrete (RC) cracking and, particularly post-cracking behavior, as one of the major sources of nonlinearity is an important and difficult task of deformation analysis. In smeared crack approach dealing with average cracking and strains, post-cracking effects can be modeled by stress-strain tension-stiffening relationships. Most of them were derived using test data of tension or shear RC members. Subsequently, these constitutive laws were applied for modeling of bending elements which behavior differs from tension or shear members. The authors have proposed an innovative 'inverse' technique for constitutive modeling of flexural RC elements. It is based on the smeared crack approach and 'layer' section model. A number of investigations have shown that the 'inverse' technique becomes a powerful tool for constitutive analysis of flexural RC members, but its computation efficiency requires an additional study. This paper discusses the computational aspects of the 'inverse' procedure and reports recommendations improving efficiency of the constitutive modeling.

Key words: Inverse analysis, constitutive modeling, numerical technique, computation efficiency, reinforced concrete, smeared crack model, flexural test.

INTRODUCTION

Civil engineers for deformation analysis of concrete structures can choose either traditional design code methods or numerical techniques. Although code methods ensure safe design, their application is limited to simple cases of structural shape and loading. Unlike code methods, the numerical techniques may take into account every physical phenomenon and as a universal tool of analysis can be applied to most complex structures. However, for some structural problems, calculation results obtained by code and numerical techniques may be controversial. Such an example is deformation analysis of lightly reinforced members subjected to short-term loading (Kaklauskas, 2001, 2004; Gribniak et al., 2008). Mainly due to chosen cracking and tension-stiffening parameters, deflections calculated by design code and finite element technique may differ over 100% (Kaklauskas, 2004; Kaklauskas et al., 2009; Gribniak, 2009).

In usual structural analysis, problems called the 'simulation' or the 'direct' ones, strength and strains (deformations) have to be defined when material properties are given. Adequate modeling of reinforced concrete (RC) cracking and, particularly post-cracking behavior, as one of the major sources of nonlinearity is the most important and difficult task of deformation analysis. Due to the bond with reinforcement, concrete between cracks carries a certain amount of the tensile force normal to the cracked plane and contributes to the overall stiffness of the structure.

In the numerical modeling, four main approaches of tension-stiffening can be distinguished: 1) stress transfer- this approach most realistically deals with the discrete cracking phenomenon. It models the bond between concrete and reinforcement bar based on the assumed bond stress-slip law; 2) fracture mechanics- cracks in concrete are modeled using the fracture mechanics principles; 3) average stress-average strain law attributed to concrete in tension; 4) average stress-average strain law attributed to tensile reinforcement.

Tension-stiffening has been widely discussed in its variety of approaches (Saliger, 1936; Hognestad, 1951; Lash, 1953; Szulczynski and Sozen, 1961; Broms, 1964; Base et al., 1966; Scanlon, 1971; Suidan and Schnobrich, 1973; Scanlon and Murray, 1974; Lin and Scordelis, 1975

---

* Corresponding author. E-mail: viktor.gribniak@vgtu.lt.

1975; Clark and Spiers, 1978; Gilbert and Warner, 1978; Somayaji and Shah, 1981; Ghali and El-Badry, 1987; Floegl and Mang, 1982; Polak and Blackwell, 1998; Gilbert, 1999, 2007; Kaklauskas, 2001, 2004; Maekawa et al., 2003; Fields and Bischoff, 2004; Scott and Beeby, 2005; Beeby and Scott, 2006; Sato et al., 2007; Scanlon and Bischoff, 2008; Vollum et al., 2008; Kaklauskas et al., 2009; Sancak, 2009; Wu and Gilbert, 2009; Büyükkaragöz, 2010; Kala et al., 2010; Bacinskas et al., 2011; Ho and Peng, 2011). Advanced numerical models of RC beams have been proposed by Rabczuk and others (Rabczuk and Eibl, 2004; Rabczuk et al., 2005, 2008; Rabczuk and Belytschko, 2007) as well as Sageresan and Drathi (2008).

The present study deals with the tension-stiffening approach attributed to tensile concrete. It is a simplified approach based on the smeared cracking conception considering an "averaged" deformation response of a cracked member. Although it is not capable of producing a realistic crack pattern, such rough idealization is very illustrative and allows a trivial quantification of the tension-stiffening effect. Based on this approach, a number of stress-strain tension-stiffening relationships have been proposed (Cervenka, 1985; Vecchio and Collins, 1986; Gupta and Maestrini, 1990; Collins and Mitchell, 1991; Hsu, 1993; Choi and Cheung, 1996; Barros et al., 2001; Bischoff, 2001; Kaklauskas and Ghaboussi, 2001; Torres et al., 2004; Ng et al., 2010).

The main deficiency concerning most known tension-stiffening relationships is that they were derived using test data of tension or shear members. Subsequently, these constitutive laws were applied for modeling of flexural elements which behavior differs from tension or shear members (Ng et al., 2010). Moreover, due to the bond with steel, tensile concrete in cracked RC structures has different properties from those that were obtained from tests of plain concrete specimens. Therefore, quite naturally a researcher is challenged to solve an 'inverse' problem in bending analysis, that is derive the material law of concrete for given moment-deflection (curvature) diagrams. Kaklauskas and Ghaboussi (2001) have formulated the principles of the 'inverse' technique for deriving tension-stiffening relationships using test data of RC flexural members. For a given moment-curvature diagram, an average stress-average strain tension-stiffening relationship was computed using the 'layer' section model. The tension-stiffening relationship was progressively derived for the extreme tension fiber of the concrete section. Recent investigations (Kaklauskas et al., 2009, 2011; Kaklauskas and Gribniak, 2011) have shown that the 'inverse' technique may serve as a powerful tool for constitutive analysis of flexural RC members. It may be relatively easy extended to other tension-stiffening approaches such as steel-related or stress transfer models. However, as was shown by Gribniak (2009), the inverse approach encounters with difficulties of a numerical character resulting in significant oscillations of

the constitutive laws under derivation. The oscillations occur mainly due to numerical peculiarities of the sensitive procedure. This paper discusses convergence of the 'inverse' procedure and reports recommendations for improving computational efficiency and robustness of the analysis.

FORMULATING INVERSE ANALYSIS

Unlike the 'direct' analysis which is used for prediction of structural response applying a specified constitutive model, the 'inverse' analysis aims at determining parameters of the model based on the response of the structure. As noted earlier, Kaklauskas and Ghaboussi (2001) have formulated the principles of the 'inverse' technique for deriving tension-stiffening relationships using the test data of RC flexural members. For a given moment-deflection/curvature diagram, a stress-strain tension-stiffening relationship was computed from the equilibrium equations of axial forces and bending moments. The 'layer' section model was employed for computation of the internal forces. The 'inverse' analysis was performed with incrementally increasing bending moment. The two equilibrium equations were solved for each loading stage yielding a solution for the coordinate of the neutral axis and the concrete stress in the extreme tension fiber. Since the extreme fiber had the maximum strain, other tension fibers of concrete had smaller strains falling within the portion of the already determined stress-strain diagram.

Approaches and assumptions

The 'inverse' analysis is based on the following approaches and assumptions:

1) Average strain, also called 'smeared crack' approach.
2) Linear strain distribution within the depth of the section implying perfect bond between layers.
3) All concrete layers in the tension zone follow a uniform stress-strain law.

Such experimental data of flexural RC members can be used for the 'inverse' technique:

i) Bending moment versus average strain of the extreme fiber of compressive concrete;
ii) Bending moment versus average strain of the extreme fiber of tensile concrete;
iii) Bending moment versus average strain of the tensile reinforcement;
iv) Bending moment versus mid-span deflection;
v) Bending moment versus curvature;
vi) Average stress versus average strain of tensile reinforcement.
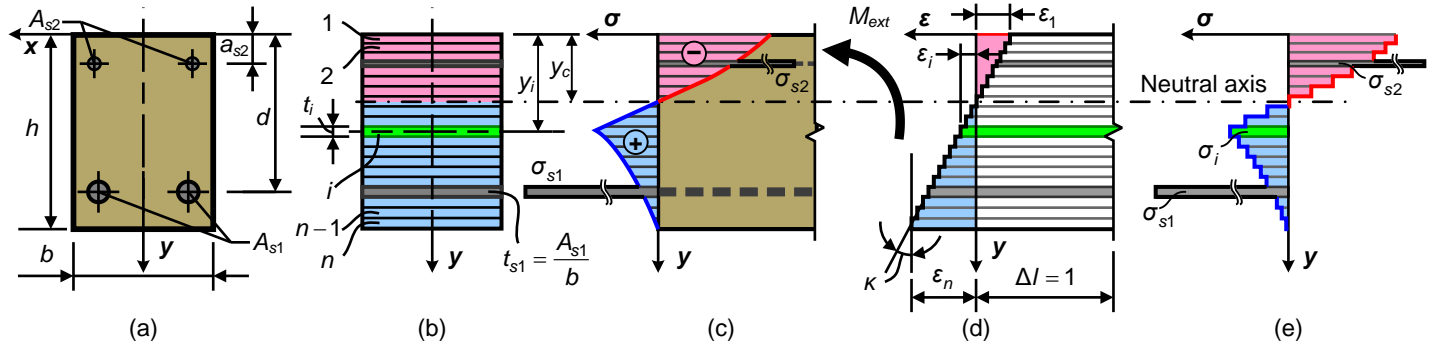
Figure 1. Layer section model.
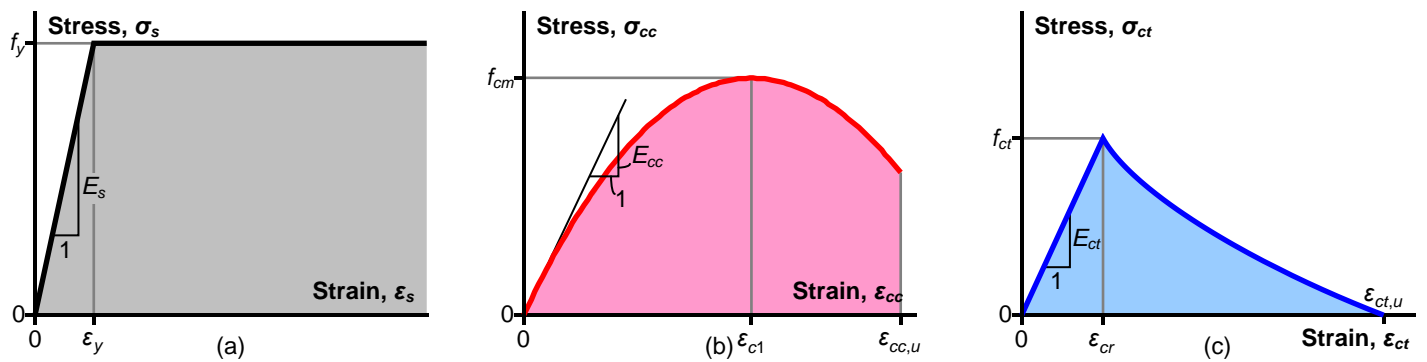
Figure 2. Constitutive laws for reinforcing steel (a), concrete in compression (b) and in tension (c).

The authors have developed an experimental procedure (Gribniak et al., 2009) for obtaining moment-curvature relations suitable for the 'inverse' analysis. The moment-curvature relations measured using the four-point-bending scheme are averaged over the pure bending zone. Such averaged moment-curvature response allows selecting a tension-stiffening model based on the smeared cracking approach. The derived model enables to simulate the same moment-curvature response as it was obtained at the tests. The 'inverse' technique combines the 'layer' section model and the 'direct' analysis technique (Kaklauskas, 2004).

Direct technique

Let us consider a doubly reinforced concrete member subjected to an external bending moment M_{ext}. A cross-section for such member is presented in Figure 1a. As shown in Figure 1b, it is divided into n layers which correspond to either reinforcement or concrete. The thickness of the reinforcement layer is taken from the condition of the equivalent area. The direct technique needs to assume material laws for reinforcement (Figure 2a) and concrete, both in compression (Figure 2b)

and tension (Figure 2c). Curvature κ and strain ε_i at any layer i (Figure 1d) can be calculated by the formulae:

$$\kappa = \frac{M_{ext}}{IE}; \quad \varepsilon_i = \kappa(y_i - y_c); \quad y_c = \frac{SE}{AE}; \quad AE = b\sum_{i=1}^{n} t_i E'_i;$$

$$SE = b\sum_{i=1}^{n} y_i t_i E'_i; \quad IE = b\sum_{i=1}^{n}\left[\frac{t_i^2}{12} + (y_i - y_c)^2\right] t_i E'_i. \quad (1)$$

Here AE, SE and IE are the area, the first and the second moments of inertia multiplied by the secant modulus E'_i. Other notations are evident from Figure 1b.

For the given strain ε_i and the constitutive law (Figure 2), the stress σ_i is obtained. Figures 1d and e illustrate strain and stress distributions within the 'layer' section model. The analysis is performed iteratively until compatibility condition between the external and internal (calculated) moments is satisfied.

Inverse technique

This study deals with the 'inverse' technique modified by Gribniak (2009). The 'inverse' analysis is based on the concept of a progressive calculation of the tension-
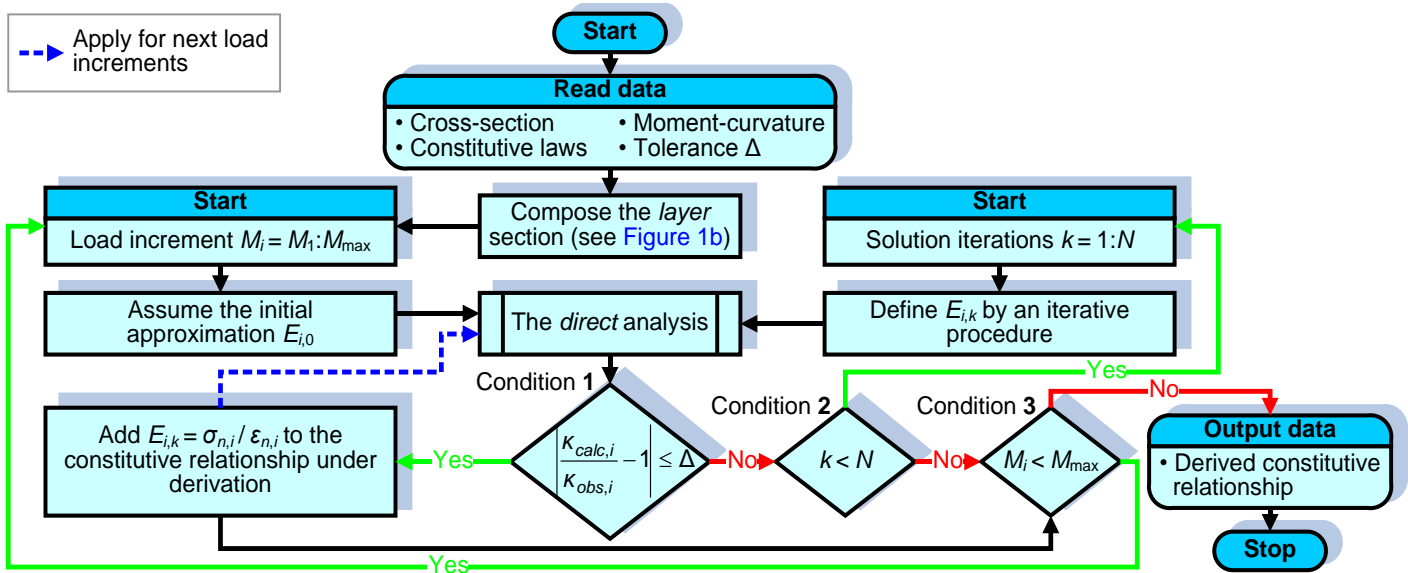
Figure 3. Flow chart of the inverse technique.

stiffening relationship for the extreme tension fiber of an RC section. The assumption of a uniform stress-strain tension-stiffening law for different layers allows reducing the dimension of the solution to a single non-linear equation. For a given load increment, an initial value of the secant deformation modulus of concrete in the extreme tensile layer is assumed and a curvature is calculated using the 'direct' technique (introduced earlier). If the calculated and experimental curvatures differ, methods of iterative analysis are used to correct the secant modulus.

Figure 3 presents a flow chart of the 'inverse' technique. Based on geometrical parameters of the cross-section, the 'layer' section model (Figure 1b) is composed. Stress-strain material laws for steel and compressive concrete are assumed (Figures 2a and b). Computations are performed iteratively for an incrementally increasing bending moment. At each moment increment i, an initial value of the secant deformation modulus of the tension-stiffening relationship under derivation is assumed. The curvature is calculated by the 'direct' technique. If the agreement between the calculated $\kappa_{calc,i}$ and the experimental $\kappa_{obs,i}$ curvatures is not within the assumed tolerance Δ, that is Condition 1 is not fulfilled (Figure 3), the analysis is repeated using an iterative procedure until Condition 2 is satisfied. At each iteration k, a secant deformation modulus $E_{i,k}$ is calculated. If the solution is found (Condition 1 is satisfied), the obtained value of $E_{i,k}$ is fixed and used for next load increments. If the limit iteration number is exceeded (k > N), the calculated $E_{i,N}$ is rejected, meaning that the deformation modulus E_i is not defined at the moment increment i and the analysis moves to the next load step. The calculation is terminated when the final loading step is reached (Condition 3).

Application of the derived tension-stiffening relationship in the 'direct' analysis would give the original moment-curvature diagram.

Iterative procedure

The 'inverse' analysis is performed according to the flow chart shown in Figure 3. For the given load increment, the initial value of the secant deformation modulus of concrete is assumed for the extreme tensile layer. Based on the 'direct' analysis, curvature is calculated. If it differs from the experimental value more than the assumed tolerance Δ, the analysis is repeated using an iterative technique. It should be noted that the required computation resources depend on the efficiency of both the 'direct' and the 'inverse' iterative algorithms. As convergence issues of the 'direct' technique were not investigated in the present study, the iteration number was limited to 100 as recommended by Kaklauskas (2001). The convergence criterion was as follows:

$$\max_{i=1...n} \left| E_{i,k} - E_{i,k-1} \right| < 10^{-4}; \quad \left| N_{int,k} \right| = \left| \sum_{i=1}^{n} A_i \sigma_{i,k} \right| < 10^{-4};$$

$$\left| M_{ext} - M_{int,k} \right| = \left| M_{ext} - \sum_{i=1}^{n} A_i y_i \sigma_{i,k} \right| < 10^{-3}. \tag{2}$$

Here, $N_{int,k}$ and $M_{int,k}$ are the internal axial force and bending moment, respectively, obtained at the k-th iteration.

Equations 2 represent requirements for convergence of the secant modulus at each layer and compatibility of

Table 1. Basic parameters of the test beams.

Beam	h (mm)	d (mm)	a_2 (mm)	b (mm)	A_{s1} (mm²)	A_{s2} (mm²)	f'$_c$ (MPa)	f$_y$ (MPa)	E$_s$ (GPa)	Age (days)	P (%)
S1-3	299	268	23	283	755	57	48.2	582	207	67	0.99
S2-3	300	272	29	282	466	57	48.1	632	211	66	0.61
S3-2-3	298	271	32	284	232	57	50.9	578	210	47	0.30

the axial forces and the bending moments. Analysis has shown that these conditions are of different weight, therefore different tolerances were used. As noted earlier, the 'inverse' analysis is based on the curvature equilibrium Condition 1 (Figure 3). The selected numerical procedure is based on the hybrid Newton-Raphson and Bisection algorithm (Gribniak, 2009) and takes into consideration recommendations reported by Kahaner et al. (1989). A secant deformation modulus of tensile concrete is defined at each of the iterations. The root (deformation modulus value) locating procedure is started using the Newton-Raphson method. For the moment increment i, the secant deformation modulus $E_{i,k}$ at the iteration k is defined:

$$E_{i,k} = E_{i,k-1} - \frac{\delta\left(E_{i,k-1}\right)}{\delta'\left(E_{i,k-1}\right)}, \quad \delta\left(E_{i,k-1}\right) = \frac{\kappa_{calc,i}}{\kappa_{obs,i}} - 1 \quad (3)$$

Here, $E_{i,k-1}$ and $\delta(E_{i,k-1})$ are, respectively, the secant deformation modulus and the curvature prediction error obtained in the previous iteration; $\delta'(E_{i,k-1})$ is the first derivation of the error obtained numerically from this central-difference equation:

$$\delta'\left(E\right) = \frac{-\delta_2 + 8\delta_1 - 8\delta_{-1} + \delta_{-2}}{12h},$$
$$\delta_2 = \delta\left(E + 2h\right); \quad \delta_1 = \delta\left(E + h\right); \quad (4)$$
$$\delta_{-1} = \delta\left(E - h\right); \quad \delta_{-2} = \delta\left(E - 2h\right).$$

Here, h is the difference grid size equal to 0.1 MPa. In the introduced equation, indices of deformation modulus E are omitted.

Using the aforementioned algorithm, only one initial approximation ($E_{l,0}$) is required. However, it requires five evaluations of the function δ(E) per iteration (Equations 3 and 4), that is the 'direct' analysis should be carried out five times what makes computations more costly. Moreover, in some cases a solution may not be found by the Newton-Raphson algorithm. Therefore, in the present study, the Newton-Raphson procedure is applied until the solution is found or root interval is determined. If the solution is found, that is Condition 1 is satisfied, the obtained value $E_{i,k}$ is fixed and used for further analysis. When the root is localized, that is

$$\delta\left(E_{i,k}\right) \cdot \delta\left(E_{i,k-1}\right) < 0 \quad (5),$$

the analysis proceeds using the Bisection method which always gives the solution if it exists. Using the Bisection method, bounds of the interval at each of the iterations approach each other until the localization interval is small enough. An important merit of the Bisection method is that the number of iterations N necessary to obtain the solution can be obtained in advance. For the given tolerance Δ, N can be obtained from the condition:

$$N \leq \left\lceil \log_2\left(\frac{E_2 - E_1}{\Delta}\right) \right\rceil, \quad E_1 < E_2 \quad (6)$$

Here the operator $\lceil x \rceil$ rounds the argument x toward the next integer number; $[E_1, E_2]$ is the root localization interval.

This method will require a single evaluation of the function δ(E) per iteration. The secant modulus is defined by the equation (Kahaner et al., 1989):

$$E_{i,k} = E_1 + \frac{E_2 - E_1}{2}, \quad [E_1, E_2] = \begin{cases} \left[E_1, E_{i,k}\right], & \delta\left(E_1\right)\delta\left(E_{i,k}\right) \leq 0; \\ \left[E_{i,k}, E_2\right], & \delta\left(E_1\right)\delta\left(E_{i,k}\right) > 0. \end{cases} \quad (7)$$

INVERSE ANALYSIS USING TEST DATA

Present analysis uses moment-curvature relationships reported by Kaklauskas and Gribniak (2011). Constitutive laws assumed in this study are shown in Figure 2. Figure 2a presents the idealized stress-strain relationship for the reinforcement, whereas Figure 2b gives the constitutive law for the compressive concrete (CEN, 2004).

Description of test data

The beams were of rectangular section with the nominal length of 3280 mm (span 3000 mm) and were tested under a four-point bending scheme with the concentrated forces dividing the span into three equal parts. In the tension zone the elements were reinforced with three deformed bars of 18, 14 and 10 mm in diameter, respectively. Stirrups in the shear span and top reinforcement were also provided. Main material characteristics listed in Table 1 are the cylinder (⌀150 × 300 mm) compressive strength of concrete f'$_c$, the yielding strength f$_y$ and the Young's modulus E$_s$ of the
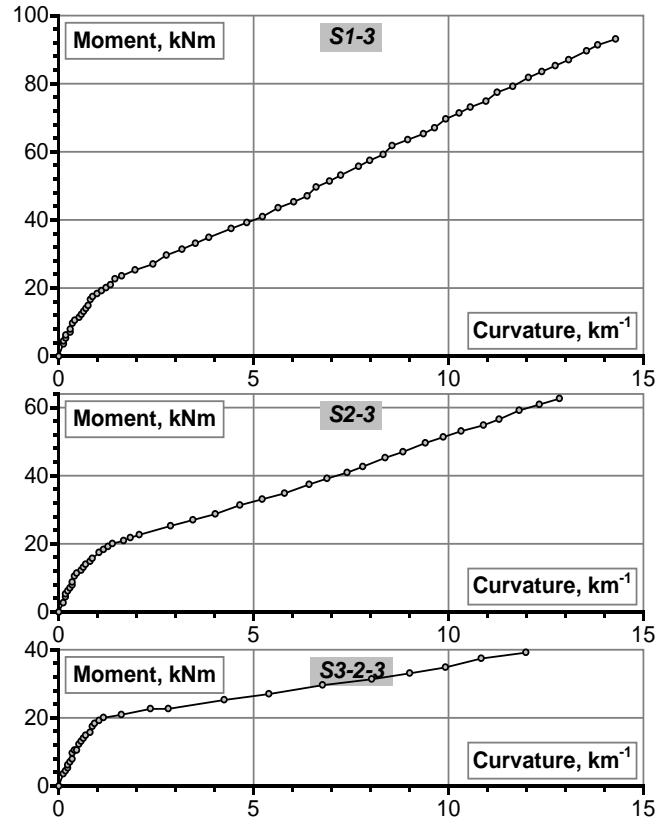
Figure 4. Moment-curvature diagrams of the test beams.

reinforcement and the reinforcement ratio $p = A_{s1}/(bd)$. Other notations are evident from Figure 1a.

Experimental moment-curvature diagrams needed for deriving tension-stiffening relationships were obtained in two ways: from deflections and from concrete surface strains, both recorded in the pure bending zone (Kaklauskas and Gribniak, 2011). Concrete surface strains were measured throughout the length of the pure bending zone on a 200 mm gauge length, using mechanical gauges. Four continuous gauge lines were located at different depths with two extreme lines placed along the top and bottom reinforcement. Measured strains were averaged along each gauge line. Tests were performed with small increments and paused for short periods (about 2 min) to take readings of gauges and to measure development of the crack. In total, it took from 40 to 60 load increments. Deflections were automatically recorded at 1 kN load increments. Good agreement was achieved between the moment-curvature diagrams obtained from deflection and strain measurements.

Present analysis is based on the data obtained from the average strains. These moment-curvature diagrams are shown in Figure 4. It should be noted that due to small load increments, the diagrams do not possess a clear horizontal part corresponding to the start of formation of major cracks.

Numerical implementation

The present analysis is based on the moment-curvature diagrams shown in Figure 4. It is important that the 'inverse' analysis is performed incrementally using the constitutive law for tensile concrete obtained at previous loading stages. This means that errors made at a given moment increment have influence on the shape of the constitutive law under derivation, particular care to avoid errors should be taken in the early stages of the analysis associated to small curvatures. Though similar in absolute terms at all loading stages, errors of curvature measurements at early stages have much higher relative effect on the derived constitutive law. Therefore, as concrete in tension prior to cracking essentially behaves elastically, a limitation on the curvature value used in the analysis has been introduced. The curvature should not be less than the calculated one by Equation 1 using elastic material parameters. If this limitation is not satisfied, it is recommended to replace the test curvature by the calculated one. To illustrate the 'inverse' technique, a detailed step-by-step numerical analysis has been performed for the beam S2-3. Let us consider load increment No 25 in the diagram shown in Figure 5a. Figure 5b presents the corresponding stress-strain relationship derived at load stages No 1 to 24. It
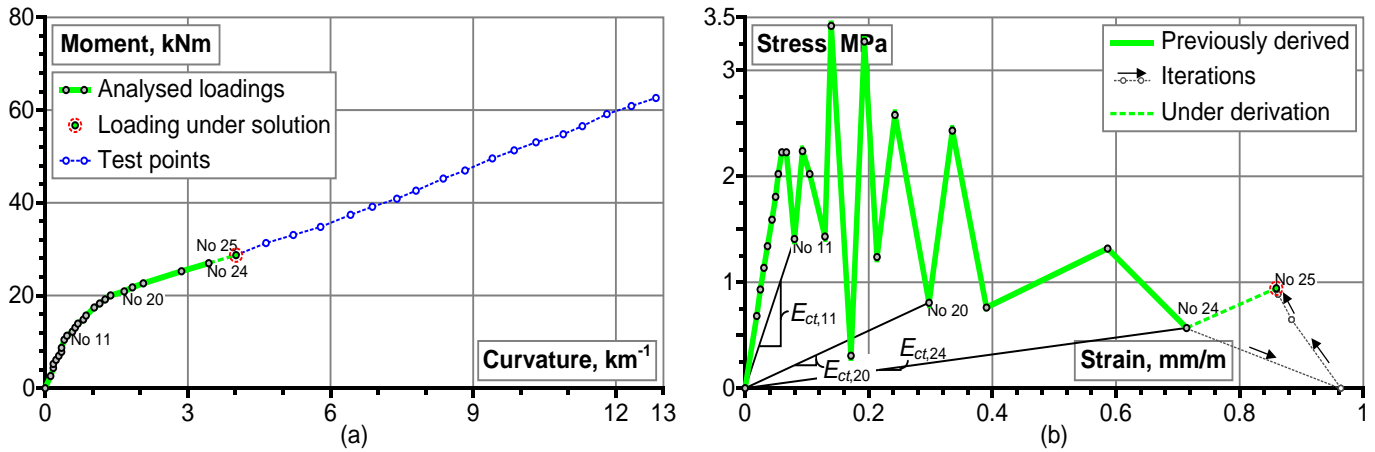
Figure 5. Solution of the inverse problem at fixed load increment.

also gives intermediate and final solution points at the load step No 25.

COMPUTATION ASPECTS OF THE INVERSE ANALYSIS

As shown in Figure 4, the analysis uses the moment-curvature diagrams of the beams S1-3, S2-3 and S3-2-3 with 57, 42 and 30 experimental points, respectively. The layer number n, the initial value of the secant modulus $E_{k,0}$ and the tolerance Δ have been considered as major parameters having influence on the convergence. In this study, two initial values of the modulus $E_{k,0} = 0$ and $E_{k,0} = E_{ct,k-1}$ (assuming the converged value from the previous load increment) were used, whereas n and Δ ranged from 40 to 1500 and from 10^{-3} to 10^{-6}, respectively. As noted earlier, at the load increment i the iterative procedure (Figure 3) may result in any of two outputs: 1) converged value of $E_{i,k}$, or 2) rejected $E_{i,N}$ (meaning that E_i was not defined). The convergence process is illustrated graphically in Figures 6, 7 and 8 where non-converged load increments are indicated by void areas. As clearly seen, the computation procedure under assumption $E_{k,0} = 0$ has reached convergence at almost all load increments. The computation assuming $E_{k,0} = E_{ct,k-1}$ is not as stable as the previous one and, in most cases, a single non-converged point causes convergence failure in the remaining load steps. After the start of cracking (that is with degrading of E_{ct}), the assumption $E_{k,0} = E_{ct,k-1}$ does not secure the convergence (Figures 6, 7 and 8). This can be explained by sensitivity of the Newton-Raphson technique with respect to the initial approximation. Therefore, further analysis uses the initial approximation $E_{k,0} = 0$.

The convergence analysis was performed for the test beams with the varying number of layers and the tolerance Δ.

The analysis results are shown in Figure 9 with the abscissa axis ("layer number, n") presented in logarithmic scale. The ordinate axis ("convergence, %") in relative terms gives a number of load increments with successful convergence of the secant modulus. It can be seen from Figure 9 that the 'inverse' procedure applied for the beam S1-3 with a higher reinforcement ratio (p = 1%) becomes extremely sensitive to a varying number of layers. The convergence effectiveness declines for the models with a layer number n greater than 300. On the other hand, stable convergence was achieved for the lightly and moderately reinforced beams (p = 0.3 and 0.6%), independently from n. Figure 9 also shows the dependence of the convergence rate on the number of layers and the tolerance Δ. The ordinate axis ("relative time") in relative terms gives the computation time in regard to the minimal time as a reference. In all cases the minimal time was obtained for minimal values of n and Δ.

Figure 9 indicates that the layer number n has the most significant influence on the computation time, whereas the tolerance effect becomes insignificant. For instance, with increased number of layers from 40 to 400, the computation time raises approximately 10 times acquiring almost linear dependence between n and the elapsed time. The tolerance has lesser effect: if it is reduced from 10^{-3} to 10^{-6}, the computation time increases less than twice.

A relative number (%) of the load steps resulting in the converged solution for ranging the tolerance Δ and the layer number n is shown in Table 2. The latter results were averaged for the three beams under consideration. It can be observed in Table 2 and Figure 9 that such input parameters as n = 140…200, $E_{k,0} = 0$ and $\Delta = 10^{-5}$ allowed to reach rational balance between the convergence success and computation time. The recommended interval of parameters Δ and n is bolded in Table 2. Further analysis assumes n = 140.

Let us consider the 'inverse' analysis procedure applied
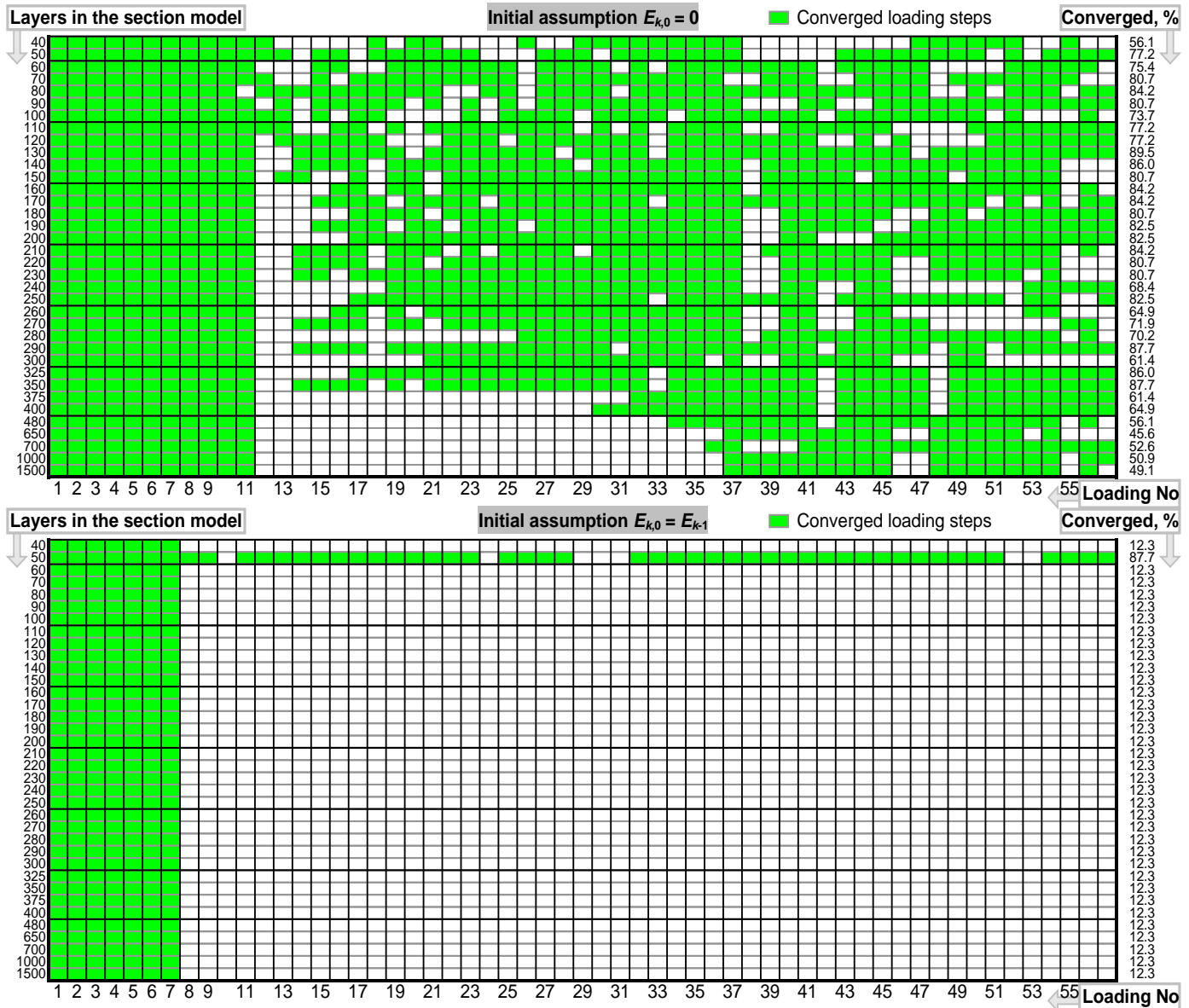
Figure 6. Convergence analysis of the beam *S1-3* under the tolerance $\Delta = 10^{-5}$ (total load steps = 57).

for the beam S1-2. The convergence was not achieved at the load steps No 12, 13, 18, 29, 38 and 55 to 57. These critical points are highlighted in Figure 10a along with corresponding curvature increment rates shown in Figure 10b. Instability of the 'inverse' procedure has two sources. The non-convergence can be explained by unstable solution processes due to changes in curvature increment rates (Figure 10b). High oscillations in the stress-strain diagram under derivation (Figure 11) usually appear at the early cracking stage and are related to sudden changes in the curvature increment rates.

Another important aspect of the analysis is an accumulative nature of the inverse procedure. Due to simplicity of the applied model, the initial oscillations

mainly caused by discrete cracking further might become dramatic. Following the assumption of a uniform constitutive law for all tensile concrete layers each sudden increment in the tension-stiffening diagram derived at the current load step should be compensated by the respective stress change of an opposite sign at the successive load steps. Such oscillations might hamper to find a solution. As can be seen in Figures 6 and 11a, the aforementioned effect is more clearly expressed in the beam S1-3 having largest amount of reinforcement. Obviously, such saw-toothed tension-stiffening relationships cannot be straightforwardly assumed as constitutive laws.

In the previous investigations (Kaklauskas and

Figure 7. Convergence analysis of the beam *S2-3* under the tolerance $\Delta = 10^{-5}$ (total load steps = 42).

Ghaboussi, 2001; Kaklauskas, 2001), the smoothing technique was based on the trial-and-error approach and involved some subjective judgment having influence on the shape of the resulting stress-strain curve. This study presents a new smoothing procedure.

TECHNIQUE FOR SMOOTHING THE OSCILLATIONS

The previous section indicates that the procedure

proposed for solving the 'inverse' problem is strongly affected by the composition of the initial data set, that is points of the moment-curvature diagram. To reduce sudden changes in curvature increment rates (as shown in Figure 10b by red circles), two data sets were formed from the experimental data. Figure 12 shows the tension-stiffening relationships derived using even and odd test points (first and second sets, respectively) of the experimental moment-curvature diagram. Only the first and the last points were used in both sets. The

Figure 8. Convergence analysis of the beam S3-2-3 under the tolerance $\Delta = 10^{-5}$ (total load steps = 30).

differences in the obtained relationships are obvious (compare Figures 10 and 12) referring to the stochastic nature of the given test data.

In order to avoid a subjective judgment, the obtained tension-stiffening relationships were smoothed using the Hardy's formula (Pollard, 1979) based on the modified running-average (MRA) method:

$$f_{i,aver} = \frac{w_0}{n} - (w_1 - 2w_0 + w_{-1})\frac{n^2 - 1}{24n^3};$$

$$w_{-1} = \sum_{i-(3n-1)/2}^{i-(n+1)/2} f_k; \quad w_0 = \sum_{i-(n-1)/2}^{i+(n-1)/2} f_k; \quad w_1 = \sum_{i+(n+1)/2}^{i+(3n-1)/2} f_k.$$

(8)

Here, $f_{i,aver}$ is the average value of i-th point; w_{-1}, w_0 and
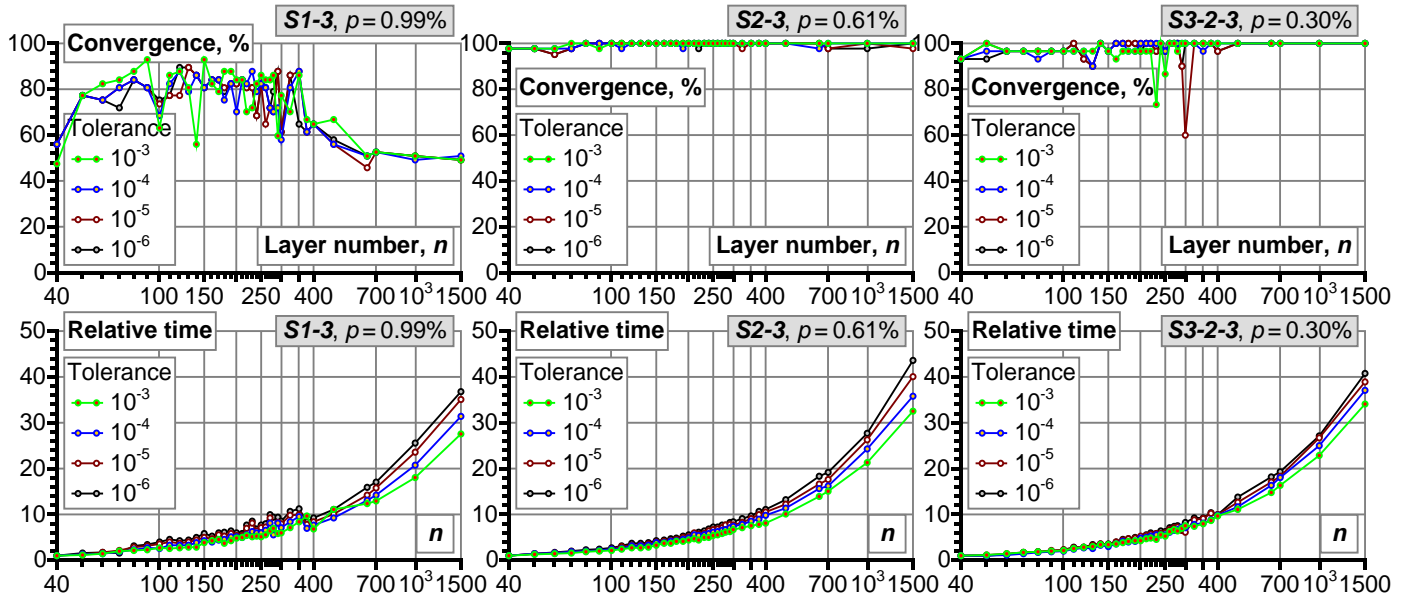
Figure 9. Analysis of computation effectiveness in respect to number of layers and the tolerance.

Table 2. Relative number of the converged load steps (%).

Tolerance	Layer number, n										
	100	**120**	**140**	**160**	**180**	**200**	**220**	**240**	**260**	**280**	**300**
$\Delta = 10^{-3}$	86.6	94.8	85.4	91.9	94.8	93.6	89.0	94.2	94.7	94.2	92.4
$\Delta = 10^{-4}$	88.4	94.8	95.3	94.7	90.7	90.1	94.2	93.0	93.6	90.1	86.0
$\Delta = 10^{-5}$	90.1	90.2	**95.3**	**94.7**	**93.6**	**94.2**	93.6	88.4	88.3	90.1	73.8
$\Delta = 10^{-6}$	90.7	94.3	95.3	94.7	93.0	93.1	92.8	89.5	93.6	90.3	87.1
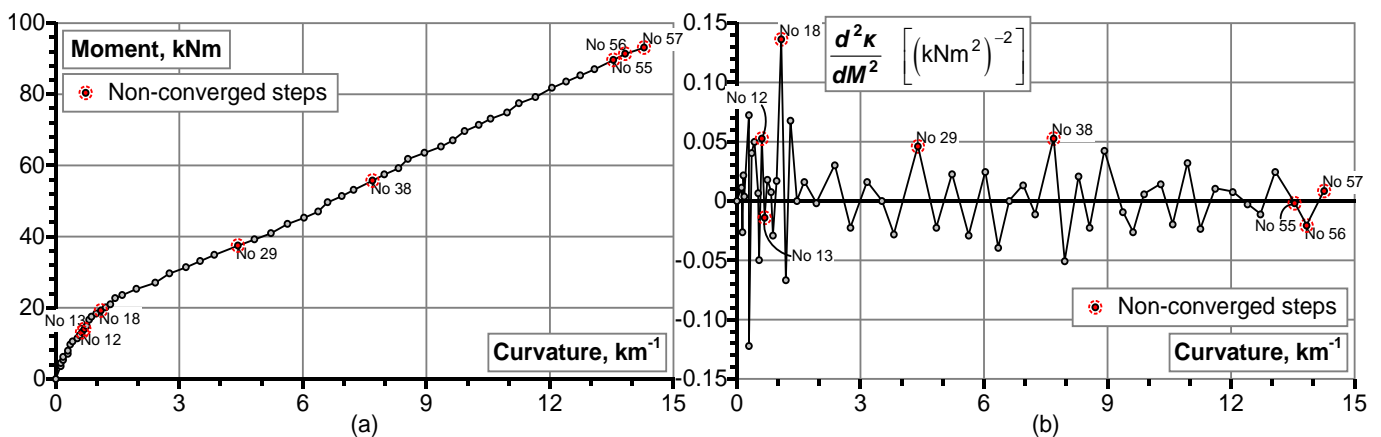
Figure 10. Curvature increment rate analysis of the beam S1-3.

w_1 are the sum of preceding, central and succeeding n ordinates; f_k is the k-th value of averaged series.

Potential of the MRA method can be exploited more extensively, if large amount of input points is used. In general, a moment-curvature diagram possesses about 20 to 30 test points only, which would restrict application
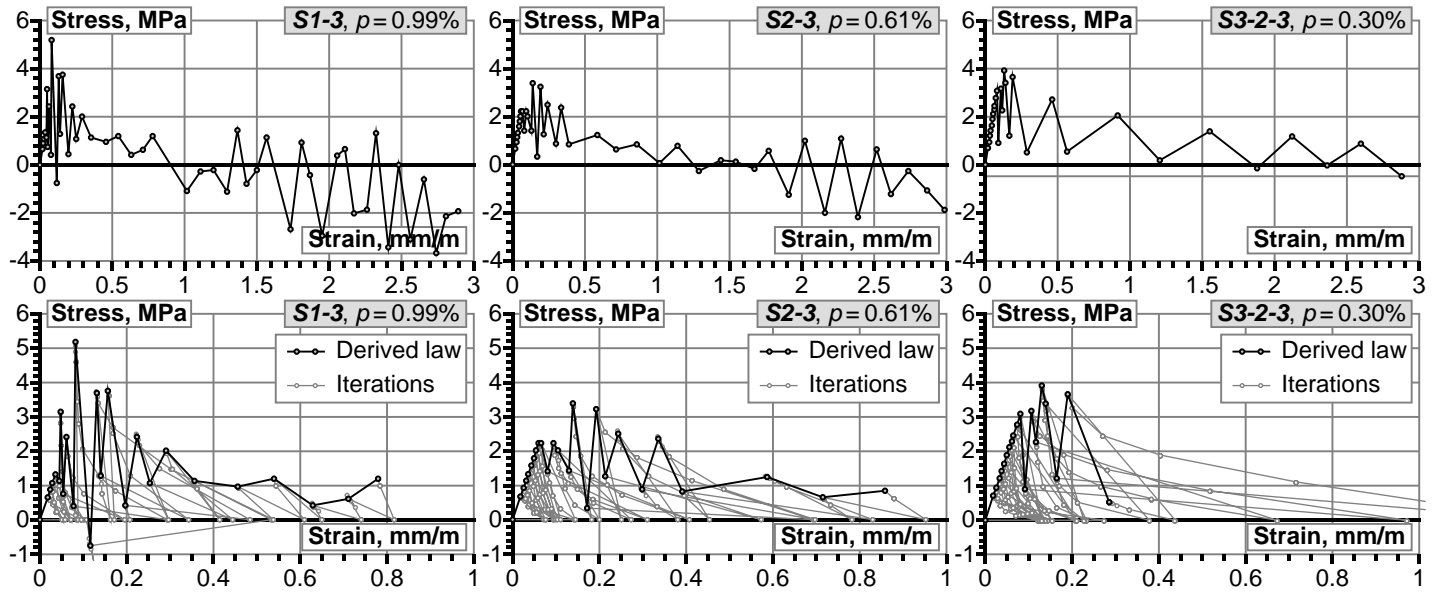
Figure 11. Derived tension-stiffening relationships (top) and fragments of these diagrams with intermediate solution steps (bottom).
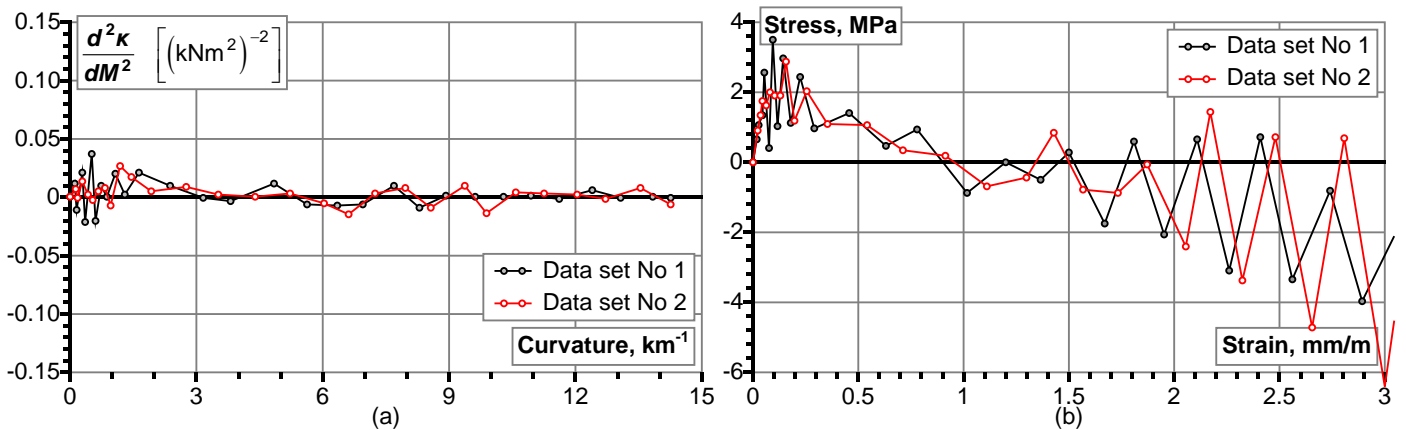
Figure 12. Variability analysis of the beam S1-3 using different data sets.

of the MRA method. To increase the amount of input data, extra pseudo-experimental data sets could be generated. Assuming that the initial data set generally has a stochastic nature, the Monte-Carlo method might be applied to form extra-data sets. It should be noted that dividing initial data into sub-sets is strongly recommended if the number of data points exceeds 80 to 100. In general, such division may be considered as additional tool for smoothing.

Using test data of the beam S1-3, multiple analyses were performed for several sets of moment-curvature data with randomly generated points. Thus, no modifications were made in the moment-curvature diagrams and, in fact, all test points were used in the analysis. In general, the effectiveness of the smoothing

procedure will increase with the larger number of sets. Various cases of composition of test data were analyzed. For illustration, some of them are given in Figure 13. As shown in Figure 13a, three data sets of moment-curvature points were generated. Sets No 1 and 2 were made using odd and even experimental points, respectively, with random introduction of extra-points. Set No 3 differs from set No 2 by a number of extra-points. The stress-strain relationships derived from the generated data sets are shown in Figure 13b. Although the stress-strain diagrams shown in Figures 12b and 13b are similar, the MRA method can be only applied for the latter data due to increased number of the points.

Figure 14 presents the smoothed tension-stiffening relationships derived for the test beams. For each of the
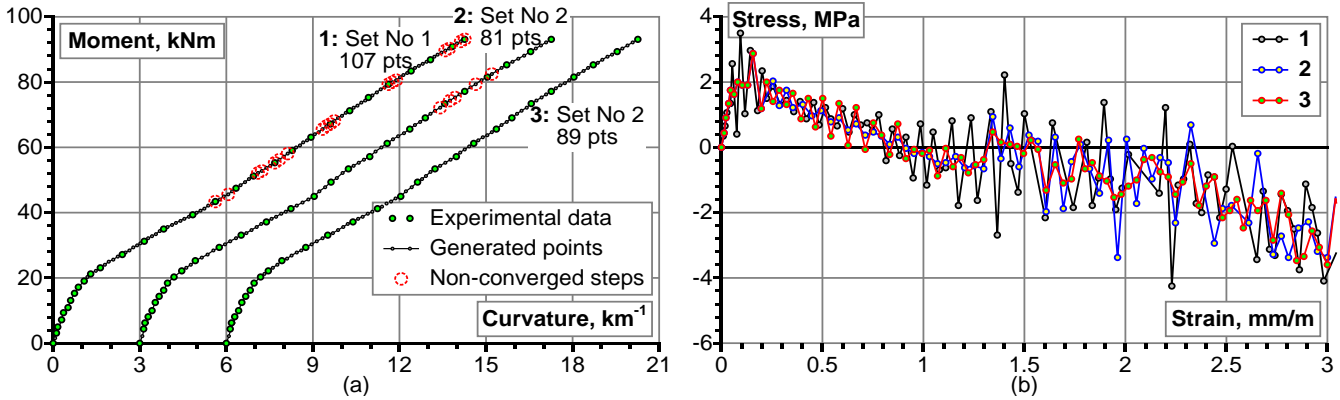
Figure 13. Monte-Carlo generation of moment-curvature points deriving stress-strain relationships of the beam S1-3.
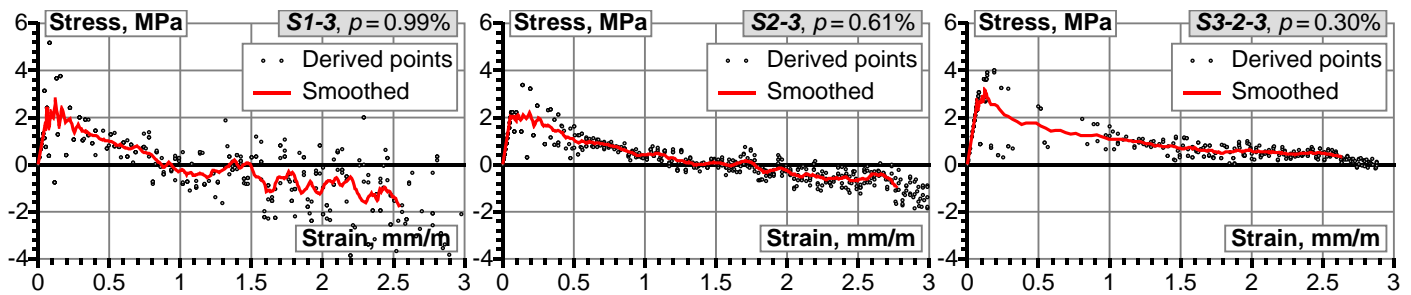
Figure 14. Smoothed stress-strain tension-stiffening relationships of the test beams.
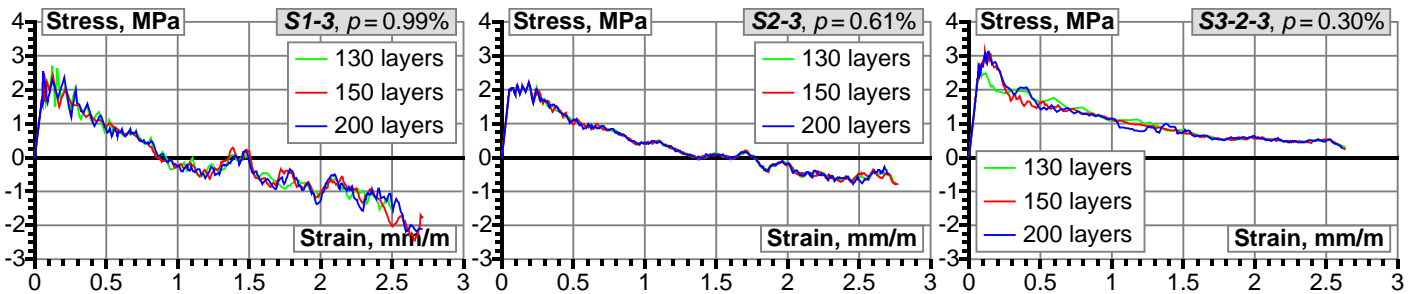
Figure 15. Smoothed tension-stiffening relationships for varying number of layers.

beams, five sets of extra moment-curvature points were generated as shown in Figure 13a. The inverse analysis was run separately for each of the sets. Further, the obtained stress-strain points were concatenated and ranged in ascending strain order. The resulting smoothed curves were given by Equation 8.

DISCUSSION OF RESULTS

For the purpose of investigating robustness of the

proposed smoothing technique, the inverse analysis was performed for each of the test beams with different number of layers in the section model. Figure 15 illustrates application of the proposed smoothing technique. This figure presents only the averaged tension-stiffening curves (without the generated inter-mediate points). It can be observed that the derived tension-stiffening curves for different number of layers have practically coincided. Some differences in the tension-stiffening curves could occur due to approximation errors, but such inaccuracies would disappear with increasing number of the generated
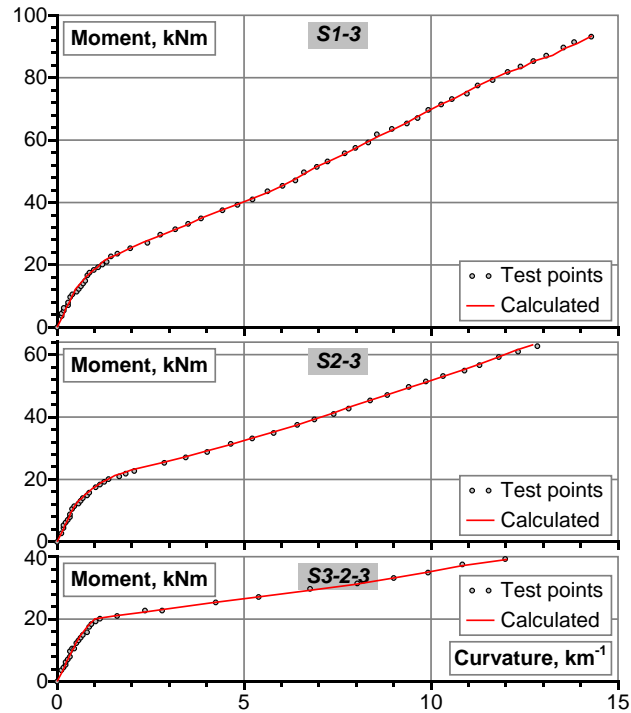
Figure 16. Calculated moment-curvature diagrams.

points. However, the amount of the inter-mediate points is limited by the capability of the 'inverse' algorithm (Figure 3) to find a solution. As shown in Figure 13a, the convergence for the beam S1-3 was not achieved at load steps highlighted by red circles. At most of these load steps, the changes in the moment-curvature diagram were not significantly different from the neighboring steps. As noted earlier, instability of the 'inverse' procedure in such cases was caused by the accumulative nature of the solution process. As the 'inverse' analysis is performed incrementally (using the portion of the constitutive law obtained at previous loading stages), each inadequate stress increment in the tension-stiffening diagram, obtained at the load step *i*, should be compensated by the respective stress change of an opposite sign at the load increment *i* + 1. Generation of excessive data points resulting in a reduction of curvature increments might restrict capability to perform this compensation, that is to find the solution. Therefore, the authors recommend generating not more than 300 points.

Adequacy of the smoothed tension-stiffening relationships shown in Figure 15 was verified using the 'layer' section model. The smoothed diagrams were employed as the constitutive laws for the non-linear curvature analysis using 200 layers. As shown in Figure 16, an excellent agreement was achieved between the predicted and the experimental curvatures.

It should be noted that the stress-strain diagrams derived for the beams S1-3 and S2-3 having larger reinforcement ratio were containing portions of negative

stresses (Figures 14 and 15). Recent investigations by the authors (Kaklauskas et al., 2008, 2009; Gribniak et al., 2009; Kaklauskas and Gribniak, 2011) indicated that the shrinkage occurring prior to the short-term loading has quite a substantial effect on deformations of RC members and the tension-stiffening relationships derived from the tests. It was shown that the obtained negative portions of the tension-stiffening curves disappear after eliminating the shrinkage effect.

The descending branches of the diagrams presented in Figures 14 and 15 characterized by the limit strain (corresponding to zero stress) were quite different for the analyzed beams. As the amount of tensile reinforcement was the only different parameter between the beams, it is expected to be responsible for the difference. In Figure 17, the derived tension-stiffening relationships were compared with a few well-known models reported in the literature. None of the latter models, excepting Gribniak (2009) were dependent on the reinforcement ratio. The ultimate strain in the simple linear tension-stiffening relationship (Gribniak 2009) was assessed by Kaklauskas and Ghaboussi (2001):

$$\varepsilon_{ct,ult} = \varepsilon_{cr} \times \max \begin{Bmatrix} 32.8 - 27.6 \cdot p + 7.12 \cdot p^2 \\ 5 \end{Bmatrix}. \tag{9}$$

Here, ε_{cr} is the cracking strain of concrete; p is the reinforcement ratio (%). Note that the ultimate strain according to Equation 9 is in good agreement with the test results (Figure 17).
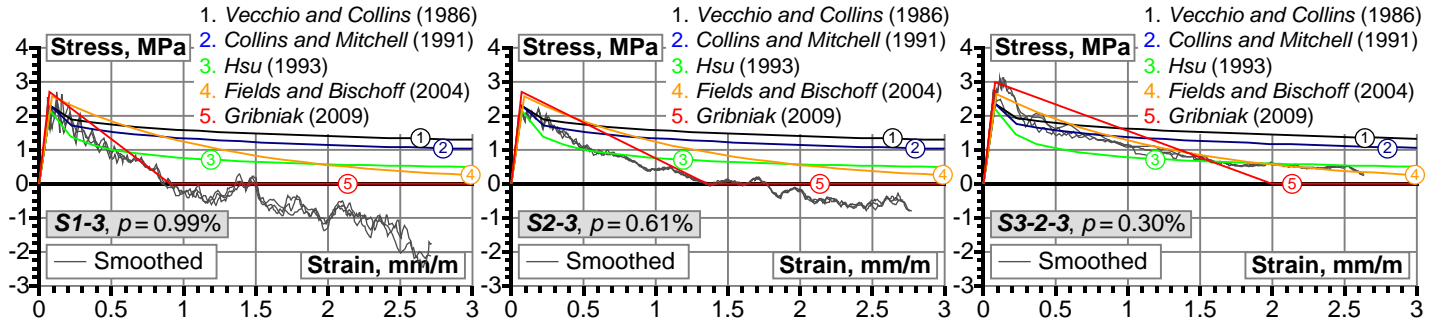
Figure 17. Comparison of tension-stiffening models.

CONCLUSIONS AND RECOMMENDATIONS

The manuscript introduces an innovative and effective computation tool solving the 'inverse' deformation problem. The 'inverse' analysis aims at determining parameters of the tension-stiffening model based on the moment-curvature response of the reinforced concrete beams. The present investigation deals with the concrete-related tension-stiffening approach based on the smeared cracking conception, that is, considers the "averaged" deformation response of a reinforced concrete member.

Using experimental data of reinforced concrete beams tested by the authors, the numerical implementation of the proposed 'inverse' procedure was analyzed, discussing the issue of the convergence. The analysis has shown that most effective results in terms of the computation time and the convergence success were achieved for the following input parameters:

i) The layer number in the section model $n = 140\ldots200$.
ii) The initial approximation of the secant modulus $E_{k,0} = 0$.
iii) The tolerance $\Delta = 10^{-5}$.

Due to discrete cracking phenomenon and accumulative nature of the 'inverse' procedure, the derived tension-stiffening relationships may have dramatic oscillations. To reduce the oscillations, an effective smoothing procedure has been proposed. The procedure is based on the following principles: 1) adjacent test points are moved into separate sets reducing sudden changes in curvature increment rates (strongly recommended, if the number of data points exceeds 80 to 100); 2) extra pseudo-experimental data points are randomly introduced by means of linear interpolation and the Monte-Carlo technique suppressing oscillations of numerical origin; 3) the resulting stress-strain relationships obtained from different simulations are averaged using the 'modified running-average' method.

The proposed technique is based on the premise that the same stress-strain relationship for cracked concrete can be used throughout the depth of the tensile zone. Although this is a convenient idealization, it is not the case in reality. The tensile stresses are transferred into the concrete through the bond at the level of the reinforcement. The assumed tension-stiffening stress-strain curve is a numerical device which has been calibrated to give good answers rather than a true representation of the mean stress distribution in the cross-section. Although it is an idealization, the assumed stress-strain relationship is perfectly reasonable and has the merit of being readily incorporated into beam and plate elements.

Further investigations are needed extending the 'inverse' analysis to other more realistic tension-stiffening approaches such as steel-related and stress transfer models. This appears to explore the cracking pattern which changes with the member depth.

REFERENCES

Bacinskas D, Kaklauskas G, Gribniak V, Sung W-P, Shih M-H (2011). Layer model for long-term deflection analysis of cracked reinforced concrete bending members. Mech. Time-Depend. Mat. (in press) DOI: 10.1007/s11043-011-9138-9.

Barros M, Martins RAF, Ferreira CC (2001). Tension stiffening model with increasing damage for reinforced concrete. Eng. Comput., 18(5-6): 759-785.

Base GL, Read JB, Beeby AW, Taylor HPJ (1966). An investigation of the crack control characteristics of various types of bar in reinforced concrete beams. Research Report 18, Cement and Concrete Association, London.

Beeby AW, Scott RH (2006). Mechanisms of long-term decay of tension stiffening. Mag. Concr. Res., 58(5): 255-266.

Bischoff PH (2001). Effects of shrinkage on tension stiffening and cracking in reinforced concrete. Can. J. Civil Eng., 28(3): 363-374.

Broms BB (1964). Stress distribution, crack patterns, and failure mechanisms of reinforced concrete members. ACI J. Proc., 61(12): 1535-1558.

Büyükkaragöz A (2010). Finite element analysis of the beam strengthened with prefabricated reinforced concrete plate. Sci. Res. Essays, 5(6): 533-544.

CEN (2004). Eurocode 2: Design of concrete structures. Part 1: General rules and rules for buildings, EN 1992-1-1:2004. Brussels: CEN.

Cervenka V (1985). Constitutive model for cracked reinforced concrete. ACI J. Proc., 82(6): 877-882.

Choi CK, Cheung SH (1996). Tension stiffening model for planar reinforced concrete members. Comput. Struct., 59(1): 179-190.

Clark LA, Speirs DM (1978). Tension stiffening in reinforced concrete beams and slabs under short-term load. Technical Report 42.521, Cement and Concrete Association, London.

Collins MP, Mitchell D (1991). Prestressed concrete structures. Englewood Cliffs, NY: Prentice-Hall Inc.

Fields K, Bischoff PH (2004). Tension stiffening and cracking of high-strength reinforced concrete tension members. ACI Struct. J., 101(4): 447-456.

Floegl H, Mang HA (1982). Tension stiffening concept based on bond slip. J. Struct. Eng.-ASCE, 108(12): 2681-2701.

Ghali A, El-Badry MM (1987). Cracking of composite prestressed concrete sections. Can. J. Civil Eng., 14(3): 314-319.

Gilbert RI (1999). Deflection calculation for RC structures – Why we sometimes get it wrong. ACI Struct. J., 96(6): 1027-1032.

Gilbert RI (2007). Tension stiffening in lightly reinforced concrete slabs. J. Struct. Eng.-ASCE, 133(6): 899-903.

Gilbert RI, Warner RF (1978). Tension stiffening in reinforced concrete slabs. J. Struct. Division-ASCE, 104(12): 1885-1900.

Gribniak V (2009). Shrinkage influence on tension-stiffening of concrete structures. PhD dissertation, Vilnius Gediminas Technical University, Vilnius, Lithuania. (Full-text access at http://www.dart-europe.eu/full.php?id=182160)

Gribniak V, Kaklauskas G, Bacinskas D (2008). Shrinkage in reinforced concrete structures: A computational aspect. J. Civil Eng. Manage., 14(1): 49-60.

Gribniak V, Kaklauskas G, Bacinskas D (2009). Experimental investigation of shrinkage influence on tension stiffening of RC beams. In: Tanabe T, Sakata K, Mihashi H, Sato R, Maekawa K, Nakamura H (eds) Creep, Shrinkage and Durability of Concrete and Concrete Structures (ConCreep 8): Proc. of the Eighth International Conference, Ise-Shima, Japan. London: CRC Press, 1: 571-577.

Gupta AK, Maestrini SR (1990). Tension-stiffness model for reinforced concrete bars. J. Struct. Eng.-ASCE, 116(3): 769-790.

Ho JCM, Peng J (2011). Strain gradient effects on flexural strength design of normal-strength concrete columns. Eng. Struct., 33(1): 18-31.

Hognestad HE (1951). Study of combined bending and axial load in reinforced concrete members. Bulletin 49, University of Illinois.

Hsu TCT (1993). Unified theory of reinforced concrete. Florida, Bocca Raton: CRC Press Inc.

Kahaner D, Moler C, Nash S (1989). Numerical methods and software. Upper Saddle River, NJ: Prentice-Hall.

Kaklauskas G (2001). Integral flexural constitutive model for deformational analysis of concrete structures. Vilnius: Technika.

Kaklauskas G (2004). Flexural layered deformational model of reinforced concrete members. Mag. Concr. Res., 56(10): 575-584.

Kaklauskas G, Ghaboussi J (2001). Stress-strain relations for cracked tensile concrete from RC beam tests. J. Struct. Eng. ASCE, 127(1): 64-73.

Kaklauskas G, Gribniak V (2011). Eliminating shrinkage effect from moment-curvature and tension-stiffening relationships of reinforced concrete members. J. Struct. Eng.-ASCE DOI: 10.1061/(ASCE)ST.1943-541X.0000395. 137(12): 1460-1469.

Kaklauskas G, Gribniak V, Bacinskas D (2008). Discussion of "Tension Stiffening in Lightly Reinforced Concrete Slabs" by R. I. Gilbert. J. Struct. Eng.-ASCE, 134(7): 1261-1262.

Kaklauskas G, Gribniak V, Bacinskas D, Vainiunas P (2009). Shrinkage influence on tension stiffening in concrete members. Eng. Struct., 31(6): 1305-1312.

Kaklauskas G, Gribniak V, Girdzius R (2011). Average stress-average strain tension-stiffening relationships based on provisions of design codes. J. Zhejiang Univ.-Sci. A, 12(10): 731-736.

Kala Z, Puklicky L, Omishore A, Karmazinova M, Melcher J (2010). Stability problems of steel-concrete members composed of high-strength materials. J. Civil Eng. Manag., 16(3): 352-362.

Lash SD (1953). Ultimate strength and cracking resistance of lightly reinforced beams. ACI J. Proc., 49(2): 573-582.

Lin CS, Scordelis AC (1975). Nonlinear analysis of RC shells of general form. J. Struct. Eng.-ASCE, 101(3): 523-538.

Maekawa K, Pimanmas A, Okamura H (2003). Nonlinear mechanics of reinforced concrete. London: Taylor & Francis Group.

Ng PL, Lam JYK, Kwan AKH (2010). Tension stiffening in concrete beams. Part 1: FE analysis. Proc. ICE Struct. Build. 163(1): 19-28.

Polak MA, Blackwell KG (1998). Modeling tension in reinforced concrete members subjected to bending and axial load. J. Struct. Eng.-ASCE, 124(9): 1018-1024.

Pollard JH (1979). A handbook of numerical and statistical techniques. Cambridge: CUP Archive.

Rabczuk T, Belytschko T (2007). A three-dimensional large deformation meshfree method for arbitrary evolving cracks. Comput. Meth. Appl. Mech. Eng., 196(29-30): 2777-2799.

Rabczuk T, Eibl J (2004). Numerical analysis of prestressed concrete beams using a coupled element free Galerkin/finite element method. Int. J. Solids Struct., 41(3-4): 1061-1080.

Rabczuk T, Akkermann J, Eibl J (2005). A numerical model for reinforced concrete structures. Int. J. Solids Struct., 42(5-6): 1327-1354.

Rabczuk T, Zi G, Bordas S, Nguyen-Xuan H (2008). A geometrically non-linear three-dimensional cohesive crack method for reinforced concrete structures. Eng. Fract. Mech., 75(16): 4740-4758.

Sageresan N, Drathi R (2008). Crack propagation in concrete using meshless method. Comput. Model. Eng. Sci., 32(2): 103-112.

Saliger R (1936). High-grade steel in reinforced concrete. Proc. of Second Congress of the International Association for Bridge and Structural Engineering (IABSE), Berlin-Munich, 1936: 293-315.

Sancak E (2009). Prediction of bond strength of lightweight concretes by using artificial neural networks. Sci. Res. Essays, 4(4): 256-266.

Sato R, Maruyama I, Sogabe T, Sogo M (2007). Flexural behavior of reinforced recycled concrete beams. J. Adv. Concr. Technol., 5(1): 43-61.

Scanlon A (1971). Time dependent deflections of reinforced concrete slabs. PhD dissertation, University of Alberta. (Full-text access at http://www.uofaweb.ualberta.ca/structures/pdfs/SER38MURRAY.pdf)

Scanlon A, Murray DW (1974). Time dependent reinforced concrete slab deflections. J. Struct. Division-ASCE, 100(9): 1911-1924.

Scanlon A, Bischoff PH (2008). Shrinkage restraint and loading history effects on deflections of flexural members. ACI Struct. J., 105(4): 498-506.

Scott RH, Beeby AW (2005). Long-term tension-stiffening effects in concrete. ACI Struct. J., 102(1): 31-39.

Somayaji S, Shah SP (1981). Bond stress versus slip relationships and cracking response of tension members. ACI J. Proc., 78(3): 217-225.

Suidan M, Schnobrich WC (1973). Finite element analysis of reinforced concrete. J. Struct. Division-ASCE, 99(10): 2109-2122.

Szulczynski T, Sozen MA (1961). Load-deformation characteristics of reinforced concrete prisms with rectilinear transverse reinforcement. Structural Research Series 224, University of Illinois.

Torres L, Lopez-Almansa F, Bozzo LM (2004). Tension-stiffening model for cracked flexural concrete members. J. Struct. Eng. ASCE, 130(8): 1242-1251.

Vecchio FJ, Collins MP (1986). The Modified Compression Field Theory for reinforced concrete elements subjected to shear. ACI Struct. J., 83(6): 925-933.

Vollum RL, Afshar N, Izzuddin BA (2008). Modelling short-term tension stiffening in tension members. Mag. Concr. Res., 60(4): 291-300.

Wu HQ, Gilbert RI (2009). Modeling short-term tension stiffening in reinforced concrete prisms using a continuum-based finite element model. Eng. Struct., 31(10): 2380-2391.